Electronic Research Archive

https://www.aimspress.com/journal/era

ERA, 32(1): 109–133.
DOI: 10.3934/era.2024006
Received: 29 October 2023
Accepted: 05 December 2023
Revised: 30 November 2023
Published: 15 December 2023

Research article

Complex nonlinear dynamics of bursting of thalamic neurons related to Parkinson's disease

Hui Zhou[1,2], **Bo Lu**[1,2,*], **Huaguang Gu**[3], **Xianjun Wang**[2] **and Yifan Liu**[2]

[1] Postdoctoral Station of Henan Institute of Science and Technology, Xinxiang 453003, China

[2] School of Mathematical Science, Henan Institute of Science and Technology, Xinxiang 453003, China

[3] School of Aerospace Engineering and Applied Mechanics, Tongji University, Shanghai 200092, China

* **Correspondence:** Email: cheersnow@163.com.

Abstract: Parkinson's disease is associated with bursting of the thalamic (TC) neuron, which receives the inhibitory synaptic current of the basal ganglia composed of multiple nuclei; deep brain stimulation (DBS) applied to the basal ganglia can eliminate the bursting to recover to the normal state. In this paper, the complex nonlinear dynamics for the appearance and disappearance of the bursting are obtained in a widely used theoretical model of a neuronal network. First, through a bifurcation analysis, isolated TC neurons exhibit paradoxical bursting induced from the resting state by enhanced inhibitory effect, which is different from the common view that the enhanced inhibitory effect should suppress the electrical behaviors. Second, the mechanism for the appearance of bursting is obtained by analyzing the electrical activities of the basal ganglia. The inhibitory synaptic current from the external segment of the globus pallidus (GPe) induces a reduced firing rate of the subthalamic nucleus (STN); then, an excitatory synaptic current from the STN induces the bursting behaviors of the GPe. The excitatory current of STN neurons and the inhibitory current of the GPe cause bursting behaviors of the internal segment of the globus pallidus (GPi), thus resulting in an enhanced inhibition from the GPi to the TC, which can induce the paradoxical bursting similar to the isolated TC neurons. Third, the cause for the disappearance of paradoxical bursting is acquired.The high frequency pulses of DBS induces enhanced firing activity of the STN and GPe neurons and enhanced inhibitory synaptic current from the GPe to the GPi, resulting in a reduced inhibitory effect from the GPi to the TC, which can eliminate the paradoxical bursting. Finally, the fast-slow dynamics of the paradoxical bursting of isolated TC neurons are acquired, which is related to the saddle-node and saddle-homoclinic orbit bifurcations of the fast subsystem of the TC neuron model. The results provide theoretical support for understanding the mechanism of Parkinson's disease and treatment methods such as DBS.

Keywords: bursting; bifurcation; Parkinson's disease; basal ganglia; thalamus

1. Introduction

Parkinson's disease (PD) is a common neurodegenerative disease caused by a dopamine deficiency in the substantia nigra of the midbrain [1, 2]. It has been found that dopamine deficiency affects the electrical activity of the striatum, which, in turn, affects the electrical activity of the network composed of the basal ganglia (BG) and the thalamic (TC) neuron. In addition to pharmacological and surgical treatments [3], deep brain stimulation (DBS), which modulates the electrical activity of the basal ganglia through high-frequency electrical stimulation [4], is also an important therapeutic tool [5, 6]. Identifying the complex dynamics of electrical activities of the thalamic and basal ganglia networks are important for understanding PD and DBS [7].

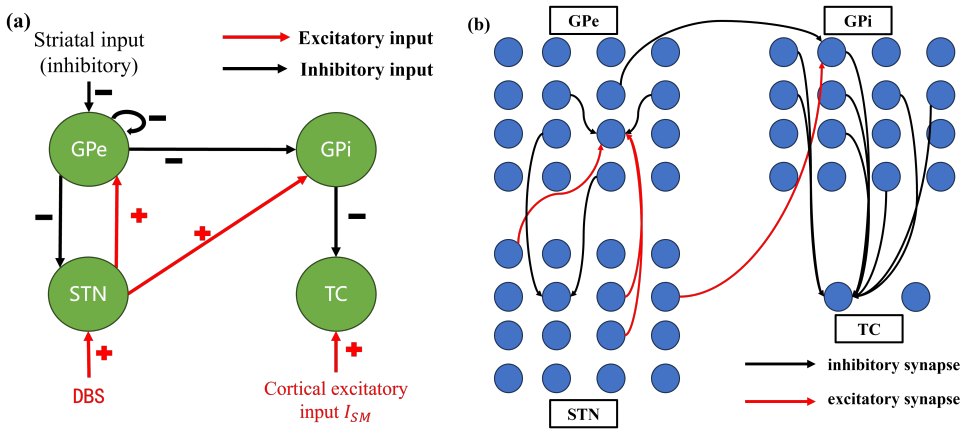

Figure 1. Topology of a network composed of basal ganglia, thalamus and cortex related to PD. (a) mapping of nuclei connectivity; (b) neuronal network connection diagram.

A network model consisting of the basal ganglia (including four nuclei: subthalamic nucleus (STN), the globus pallidus (GPe), the internal segment of the globus pallidus (GPi), and the striatum), TC and cortex has been widely used to study PD [8, 9], as shown in Figure 1. The "+" represents the excitatory effect and the "-" represents the inhibitory effect. The effect of the striatum is treated as a constant negative current acting on the GPe, and the cortical effect on the thalamus is modeled as a periodic positive pulse current. In the normal state, the thalamus faithfully responds to incoming sensorimotor signals (pulse stimulations) from the cortex, that is, each sensorimotor signal induces one action potential of the thalamus, which turns into a PD state when the thalamus is no longer able to faithfully relay the sensorimotor input [10]. For example, some sensorimotor signals induce bursting of the thalamus. When DBS is applied to the STN, its subsequent firing will be enhanced. The increased firing rate of the STN will lead to an increase in GPe firing and a decrease in GPi firing. Consequently, this reduction in the inhibitory effect from the GPi to the TC will result in the cessation of thalamic bursting and the restoration of firing corresponding to pulse stimulation. This signifies the therapeutic effect in the context of PD. Although recent studies have begun to model the striatum and cortex to study β-oscillations related to PD [11], thalamic firing, especially bursting, remains an important indicator of

PD. It is well known that bursting in the nervous system is associated with numerous brain functions and brain disorders [12–15]. In general, the generation of bursting involves complex fast-slow variables and numerous bifurcations, which are regulated by multiple factors [16–20]. Therefore, revealing the mechanism of bursting generation in the thalamus is important for understanding and treating of PD.

On one hand, thalamic bursting can be induced by positive impulse stimulation, which is in line with conventional knowledge that positive impulse stimulation enhances firing [21]. On the other hand, thalamic bursting could also be induced by inhibitory synaptic currents from GPi via the post inhibitory rebound (PIR) mechanism. PIR is a paradoxical phenomenon in which inhibitory pulse stimulation induces firing associated with a variety of brain functions or disorders [22–27]. Theoretically, PIR is related to the Hopf bifurcation and the saddle-node bifurcation on an invariant cycle. In neurophysiology, PIR is related to the either T-type calcium current or hyperpolarization-activated cation current. Experimentally, TC neurons have been found to produce bursting after receiving inhibitory currents [28] and is mediated by T-type calcium currents [29]. In addition to the PIR, recent experimental and theoretical studies have found many other paradoxical phenomena such as the enhancement of bursting induced by inhibitory effects and the reduction of bursting induced by excitatory effects [18, 30–34]. Furthermore, the intricate bifurcations of these paradoxical bursts are uncovered by dissecting the fast and slow variables [16, 35–37]. This provides novel theoretical insights into the bursting phenomenon and its modulation mechanisms. To date, there are relatively few studies on the fast-slow variable dissection for multiple types of bursting in mathematical models of the thalamic neurons, and there are few analyses of the fast-slow variable dissection variables for PIR bursting. Consequently, it becomes crucial to investigate whether the bursting of thalamic neurons is triggered by positive impulses, is induced by the PIR mechanism, or is associated with complex bifurcations. Such investigations hold great significance in deepening our understanding of PD and exploring effective therapeutic methodologies.

In this paper, for the model of the coupled system shown in Figure 1(a), we simulated the firing activities within the network level corresponding to PD and DBS treatments. By combining the bifurcations of isolated thalamic neurons, we found that the occurrence of thalamic bursting in relation to PD is not triggered by PIR but is induced by inhibitory synaptic currents. This finding challenges the conventional belief that negative currents suppress neuronal firing. Furthermore, our study also examined the responses of isolated neurons and those receiving different types of inhibitory and excitatory synaptic currents within the neural network, as well as the dissection of fast-slow variables. The inhibitory synaptic current of the GPi in the network to the thalamic neurons was the reason for the paradoxical bursting of TC neurons in the network. After the stimulation of the STN by DBS, the inhibitory synaptic current disappeared through the network dynamics, which led to the disappearance of the abnormal bursting of TC neurons. Moreover, the fast-slow dynamics and the bifurcation mechanism of the paradoxical bursting in the TC neurons were further revealed. The results of this study revealed the dynamics of the paradoxical bursting of thalamic neurons and provided a new viewpoint on the thalamic bursting associated with PD, which can help to understand the treatment of PD and DBS.

2. Network models and methods

The neuron and network models used in this paper are from the literature [9], which have been widely used to study electrical activity associated with PD.

2.1. Single neuron model

2.1.1. Neuronal model of the thalamic neurons

The thalamic neuron is modeled as follows:

$$C\frac{\mathrm{d}V}{\mathrm{d}t} = \sum_{\mathrm{TC}} I = -I_L - I_{Na} - I_K - I_T + I_{SM} + I_{app} \tag{2.1a}$$

$$\frac{\mathrm{d}h}{\mathrm{d}t} = \frac{h_\infty(V) - h(V)}{\tau_h(V)} \tag{2.1b}$$

$$\frac{\mathrm{d}r}{\mathrm{d}t} = \frac{r_\infty(V) - r(V)}{\tau_r(V)} \tag{2.1c}$$

The three variables are membrane potential V, the inactivation variable for sodium channel h, and the inactivation gating variable related to the low threshold calcium current r. $I_L = g_L(V - E_L)$, $I_{Na} = g_{Na}m_\infty^3 h(V - E_{Na})$, $I_K = g_K(0.75(1-h)^4)(V - E_K)$ and $I_T = g_T p_\infty^2 r(V - E_T)$ represent the leakage current, the sodium current, the potassium current, and the low-threshold T-calcium current, respectively. I_{SM} represents sensorimotor input current from the cortex, and I_{app} is an external constant current used to regulate the firing of neurons. C represents the membrane capacitance of the neuron. τ_h and τ_r represent the time constants of I_{Na} and I_T, respectively. g_L, g_{Na}, g_K and g_T are the corresponding maximum conductances, and E_L, E_{Na}, E_K and E_T are the corresponding reversal potentials. The expressions for the functions m_∞, h_∞, p_∞ and r_∞ are $m_\infty = \frac{1}{1+\exp\left(-\frac{V+37}{7}\right)}$, $h_\infty = \frac{1}{1+\exp\left(\frac{V+41}{4}\right)}$, $p_\infty = \frac{1}{1+\exp\left(-\frac{V+60}{6.2}\right)}$ and $r_\infty = \frac{1}{1+\exp\left(\frac{V+84}{4}\right)}$, respectively. The time constants τ_r and τ_h are expressed as follows: $\tau_r = 28+\exp(-\frac{V+25}{10.5})$ and $\tau_h = \frac{1}{0.128\exp(-\frac{V+46}{18})+\frac{4}{1+\exp(-\frac{V+23}{5})}}$.

The parameter values of the TC model are as follows: $C = 1\,\mu\mathrm{F/\,cm^2}$, $g_L = 0.05\,\mathrm{mS/cm^2}$, $E_{_L} = -70\,\mathrm{mV}$, $g_{Na} = 3\,\mathrm{mS/cm^2}$, $E_{_{Na}} = 50\,\mathrm{mV}$, $g_K = 5\,\mathrm{mS/cm^2}$, $E_K = -90\,\mathrm{mV}$, $g_T = 5\,\mathrm{mS/cm^2}$, $E_T = 0\,and\mathrm{mV}$.

2.1.2. Subthalamic nucleus (STN) model

The subthalamic nucleus (STN) is modeled as follows:

$$\frac{\mathrm{d}V}{\mathrm{d}t} = \sum_{\mathrm{STN}} I = -I_L - I_{Na} - I_K - I_T - I_{Ca} - I_{AHP} + I_{DBS} + I_{app} \tag{2.2a}$$

$$\frac{\mathrm{d}n}{\mathrm{d}t} = \phi_n\frac{n_\infty(V) - n(V)}{\tau_n(V)} \tag{2.2b}$$

$$\frac{\mathrm{d}h}{\mathrm{d}t} = \phi_h\frac{h_\infty(V) - h(V)}{\tau_h(V)} \tag{2.2c}$$

$$\frac{\mathrm{d}r}{\mathrm{d}t} = \phi_r\frac{r_\infty(V) - r(V)}{\tau_r(V)} \tag{2.2d}$$

$$\frac{\mathrm{d}Ca}{\mathrm{d}t} = \varepsilon(-I_{Ca} - I_T - k_{Ca}\cdot Ca) \tag{2.2e}$$

There are five variables in this model: the voltage variable V, the activation variable of the potassium channel n, the activation variable of sodium channel h, the inactivation gating variable related to low

threshold calcium currents r, and the calcium-activated potassium gating variable for the calcium-activated potassium current Ca. $I_L = g_L(V - E_L)$, $I_{Na} = g_{Na}m_\infty^3 h(V - E_{Na})$, $I_K = g_K n^4(V - E_K)$, $I_T = g_T a_\infty^3 b_\infty^2(V - E_{Ca})$, $I_{Ca} = g_{Ca}s_\infty^2(V - E_{Ca})$, and $I_{AHP} = g_{AHP}(V - E_K)(Ca/(Ca + k_1))$ represent the leakage current, the sodium current, the potassium current, the low-threshold T-calcium current, the calcium current, and the calcium-activated potassium ion current, respectively. I_{app} represents the external excitation current, usually expressed as a constant current, which is used to regulate the neuron's firing behavior; I_{DBS} is the periodic current acting on the STN, which is used to change the neuron's firing frequency. C represents the capacitance of the neuron, τ_h, τ_n and τ_r represent the time constant of I_{Na}, I_K and I_T current, respectively. g_L, g_{Na}, g_K, g_T, g_{Ca} and g_{AHP} are the corresponding maximum conductances, and E_L, E_{Na}, E_K, and E_{Ca} are the corresponding reversal potentials. The functions m_∞, n_∞, a_∞, s_∞, h_∞, r_∞ and b_∞ are expressed as $m_\infty = \frac{1}{1+\exp\left(-\frac{V+30}{15}\right)}$, $n_\infty = \frac{1}{1+\exp\left(-\frac{V+32}{8}\right)}$, $a_\infty = \frac{1}{1+\exp\left(-\frac{V+63}{7.8}\right)}$, $s_\infty = \frac{1}{1+\exp\left(-\frac{V+39}{8}\right)}$, $h_\infty = \frac{1}{1+\exp\left(\frac{V+39}{3.1}\right)}$, $r_\infty = \frac{1}{1+\exp\left(\frac{V+67}{2}\right)}$ and $b_\infty = \frac{1}{1+\exp\left(\frac{r-0.4}{-0.1}\right)} - \frac{1}{1+\exp(4)}$, respectively. The time constant functions τ_h, τ_n, and τ_r are $\tau_h = 1 + \frac{500}{1+\exp\left(\frac{V+57}{3}\right)}$, $\tau_n = 1 + \frac{100}{1+\exp\left(\frac{V+80}{26}\right)}$, and $\tau_r = 40 + \frac{17.5}{1+\exp\left(\frac{V-68}{2.2}\right)}$, respectively.

The parameter values for the STN model are as follows: $C = 1\,\mathrm{pF}/\mu\mathrm{m}^2$, $g_L = 2.25\,\mathrm{mS/cm}^2$, $g_{Na} = 37.5\,\mathrm{mS/cm}^2$, $g_K = 45\,\mathrm{mS/cm}^2$, $g_T = 0.5\,\mathrm{mS/cm}^2$, $g_{Ca} = 0.5\,\mathrm{mS/cm}^2$, $g_{AHP} = 9\,\mathrm{mS/cm}^2$, $E_L = -60\,\mathrm{mV}$, $E_{Na} = 55\,\mathrm{mV}$, $E_K = -80\,\mathrm{mV}$, $E_{Ca} = 140\,\mathrm{mV}$, $\phi_n = 0.75$, $\phi_h = 0.75$, $\phi_r = 0.2$, $\varepsilon = 3.75 \times 10^{-5}$, and $k_1 = 15$, $k_{Ca} = 22.5$.

2.1.3. The external segment of the globus pallidus (GPe) and internal segment of the globus pallidus (GPi) model

The GPe and GPi models are identical, except for the external stimulus current I_{app}. The model is as follows:

$$C\frac{\mathrm{d}V}{\mathrm{d}t} = \sum_{GPe/GPi} I = -I_L - I_{Na} - I_K - I_T - I_{Ca} - I_{AHP} + I_{app} \tag{2.3a}$$

$$\frac{\mathrm{d}n}{\mathrm{d}t} = \phi_n \frac{n_\infty(V) - n(V)}{\tau_n(V)} \tag{2.3b}$$

$$\frac{\mathrm{d}h}{\mathrm{d}t} = \phi_h \frac{h_\infty(V) - h(V)}{\tau_h(V)} \tag{2.3c}$$

$$\frac{\mathrm{d}r}{\mathrm{d}t} = \phi_r \frac{r_\infty(V) - r(V)}{\tau_r(V)} \tag{2.3d}$$

$$\frac{\mathrm{d}Ca}{\mathrm{d}t} = \varepsilon(-I_{Ca} - I_T - k_{Ca}Ca) \tag{2.3e}$$

The model has five variables: the membrane potential V, the activation variable of potassium channel n, the inactivation variable of sodium channel h, the inactivation gating variable related to low-threshold calcium current r, and the gating variable related to calcium-activated potassium current Ca. $I_L = g_L(V-E_L)$, $I_{Na} = g_{Na}m_\infty^3 h(V-E_{Na})$, $I_K = g_K n^4(V-E_K)$, $I_T = g_T a_\infty^3 r(V-E_{Ca})$, $I_{Ca} = g_{Ca}s_\infty^2(V-E_{Ca})$, and $I_{AHP} = g_{AHP}(V-E_K)(Ca/(Ca+k_1))$ represent the leakage current, the sodium current, the potassium current, the low-threshold T-calcium current, the calcium current, and the calcium-activated potassium current, respectively. I_{app} represents the external excitation current used to modulate the neuronal firing behavior. To more closely match the experiment, the I_{app} for the GPi is higher than the I_{app} for the GPe.

C represents the capacitance of the neuron, τ_h, τ_n, and τ_r represent the time constant of the I_{Na}, I_K, and I_T currents, respectively. g_L, g_{Na}, g_K, g_T, g_{Ca}, and g_{AHP} are the corresponding maximum conductances, and E_L, E_{Na}, E_K and E_{Ca} are the corresponding reversal potentials. The functions m_∞, s_∞, a_∞, n_∞, h_∞ and r_∞ have the following expressions: $m_\infty = \frac{1}{1+\exp\left(-\frac{V+37}{10}\right)}$, $n_\infty = \frac{1}{1+\exp\left(-\frac{V+50}{14}\right)}$, $a_\infty = \frac{1}{1+\exp\left(-\frac{V+57}{2}\right)}$, $s_\infty = \frac{1}{1+\exp\left(-\frac{V+35}{2}\right)}$, $h_\infty = \frac{1}{1+\exp\left(\frac{V+58}{12}\right)}$, and $r_\infty = \frac{1}{1+\exp\left(\frac{V+70}{2}\right)}$. The time constants τ_h, τ_n, and τ_r are as follows: $\tau_h = 0.05 + \frac{0.27}{1+\exp\left(-\frac{V+40}{12}\right)}$, $\tau_n = 0.05 + \frac{0.27}{1+\exp\left(-\frac{V+40}{12}\right)}$, and $\tau_r = 30$.

The parameter values used for the GPe and GPi neuron models are as follows: $C = 1\,\mathrm{pF}/\mu\mathrm{m}^2$, $g_L = 0.1\,\mathrm{mS/cm}^2$, $g_{Na} = 120\,\mathrm{mS/cm}^2$, $g_K = 30\,\mathrm{mS/cm}^2$, $g_T = 0.5\,\mathrm{mS/cm}^2$, $g_{Ca} = 0.15\,\mathrm{mS/cm}^2$, $g_{AHP} = 30\,\mathrm{mS/cm}^2$, $E_{_L} = -55\,\mathrm{mV}$, $E_{_{Na}} = 55\,\mathrm{mV}$, $E_K = -80\,\mathrm{mV}$, $E_{Ca} = 120\,\mathrm{mV}$, $\phi_n = 0.1$, $\phi_h = 0.05$, $\phi_r = 1$, $\varepsilon = 1 \times 10^{-4}$, $k_1 = 30$, $k_{Ca} = 15$, $I_{app} = 2.2\,\mu\mathrm{A/cm}^2$ in GPe neurons and $I_{app} = 3\,\mu\mathrm{A/cm}^2$ in GPi neurons. Because GPe receives inhibitory action from the striatum, the GPe is chosen to be $I_{app} = 2.2\,\mu\mathrm{A/cm}^2$, which is lower than the GPi.

2.2. Network model

2.2.1. Coupling

The network model shown in Figure 1(a) contains 16 STN neurons, 16 GPe neurons, 16 GPi neurons, and two TC neurons. Each STN neuron received inhibitory inputs from 2 GPe neurons. Each GPe neuron received excitatory inputs from three STN neurons. Each GPi received excitatory inputs from one STN neuron and inhibitory inputs from two GPe neurons. Each TC neuron received inhibitory inputs from eight GPi neurons. Each GPe neuron received inhibitory inputs from two other GPe neurons, as shown in Figure 1(b).

2.2.2. Network models

$$C\frac{\mathrm{d}V_{TC}}{\mathrm{d}t} = \sum_{TC} I + I_{GPi\to TC} + I_{SM} \tag{2.4a}$$

$$C\frac{\mathrm{d}V_{STN}}{\mathrm{d}t} = \sum_{STN} I + I_{GPe\to STN} + I_{DBS} \tag{2.4b}$$

$$C\frac{\mathrm{d}V_{GPe}}{\mathrm{d}t} = \sum_{GPe} I + I_{GPe\to GPe} + I_{STN\to GPe} \tag{2.4c}$$

$$C\frac{\mathrm{d}V_{GPi}}{\mathrm{d}t} = \sum_{GPi} I + I_{GPe\to GPi} + I_{STN\to GPi} \tag{2.4d}$$

$V_{_{TC}}$, $V_{_{STN}}$, $V_{_{GPe}}$, and $V_{_{GPi}}$ represent the membrane potentials of TC, STN, GPi, and GPe neurons, respectively. $I_{GPi\to TC}$ represents the inhibitory synaptic currents received by the thalamus from GPi, and I_{SM} represents the excitatory input from the cortex to thalamus. $I_{GPe\to STN}$ represents the inhibitory synaptic current from the GPe to the STN, and I_{DBS} represents the positive and high-frequency stimulation applied to the STN. $I_{GPe\to GPe}$ represents the inhibitory synaptic current from the GPe neuron to the other GPe neurons, and $I_{STN\to GPe}$ represents the excitatory synaptic current from the STN to the GPe. $I_{GPe\to GPi}$ represents the inhibitory synaptic current from the GPe to the GPi, and $I_{STN\to GPi}$ is excitatory

synaptic current from the STN to the GPi. It should be noted that each model of the network should be given a subscript to show the number of neurons; however, the models with subscripts look more complex, the model descriptions in this paper are relatively simple to be easily understood.

The excitatory input from the cortex to the thalamus I_{SM} is a periodic pulse current (see the second half of the red solid line in Figure 6), and the function is $I_{SM} = i_{SM}H(\sin(2\pi t/\rho_{SM}))\times[1-H(\sin(2\pi(t+\delta_{SM})/\rho_{SM}))]$, where H is the Heaviside function:

$$H(x) = \begin{cases} 0, & x < 0 \\ 0.5, & x = 0 \\ 1, & x > 1 \end{cases}$$

ρ_{SM}, δ_{SM}, and i_{SM} are the period, the duration, and the amplitude of the pulse, respectively.

I_{DBS} is the high-frequency pulse current applied to the STN and the deep brain stimulation (see the second half of the red solid line in Figure 7(a)), and the function is $I_{DBS} = i_{DBS}H(\sin(2\pi t/\rho_{DBS}))\times[1-H(\sin(2\pi(t+\delta_{DBS})/\rho_{DBS}))]$, where H is the Heaviside function, ρ_{DBS} is the period of the pulse, δ_{DBS} is the pulse duration, and i_{DBS} is the amplitude.

2.2.3. Synapse model

The synaptic current function is expressed as $I_{\alpha\to\beta} = g_{\alpha\to\beta}(V_\beta - E_{\alpha\to\beta})\sum_j s_\alpha^j$, where α represents a presynaptic neuron, β denotes a postsynaptic neuron, $I_{\alpha\to\beta}$ represents the synaptic current from the presynaptic neuron α to the postsynaptic neuron β, $g_{\alpha\to\beta}$ is the maximum synaptic conductance, V_α is the membrane potential of the presynaptic neuron, V_β is the membrane potential of the postsynaptic neuron, $E_{\alpha\to\beta}$ is the inverse synaptic potential, j represents the number of presynaptic neurons and $\sum_j s_\alpha^j$ corresponds to the sum of the gating variables of the j presynaptic neurons. The expression of the s function is as follows:

$$\frac{\mathrm{d}s_\alpha}{\mathrm{d}t} = A_\alpha(1-s_\alpha)H(V_\alpha-\theta_\alpha) - B_\alpha s_\alpha \tag{2.5a}$$

H is the Heaviside function, A_α and B_α denote the rate of activation and deactivation of the synaptic currents,respectively,and θ_α is the synaptic threshold of the presynaptic neuron (a presynaptic neuron with a membrane potential higher than θ_α induce the synapse activated). The parameters of the synaptic variable s_α and the synaptic current $I_{\alpha\to\beta}$ in the network are shown in Tables 1 and 2.

Table 1. Parameters of synapses in the network.

A_α	B_α	θ_α
$A_{GPi} = 2$	$B_{GPi} = 0.08$	$\theta_{GPi} = -20$
$A_{GPe} = 1$	$B_{GPe} = 0.1$	$\theta_{GPe} = -20$
$A_{STN} = 1$	$B_{STN} = 0.05$	$\theta_{STN} = -30$

Table 2. Parameters of synaptic connections between individual neurons in the network.

Synaptic current ($\mu A/cm^2$)	Conductance (mS/cm^2)	Reversal potential (mV)
$I_{GPe\to STN}$	$g_{GPe\to STN} = 0.9$	$E_{GPe\to STN} = 0.9$
$I_{STN\to GPe}$	$g_{STN\to GPe} = 0.3$	$E_{STN\to GPe} = 0.3$
$I_{GPe\to GPe}$	$g_{GPe\to GPe} = 1$	$E_{GPe\to GPe} = 1$
$I_{STN\to GPi}$	$g_{STN\to GPi} = 0.3$	$E_{STN\to GPi} = 0.3$
$I_{GPe\to GPi}$	$g_{GPe\to GPi} = 0.75$	$E_{GPe\to GPi} = 0.7$
$I_{GPi\to TC}$	$g_{GPi\to TC} = 0.1$	$E_{GPi\to TC} = 0.1$

2.3. Fast-slow variable dissection to the bursting of thalamic neurons

In the thalamic neuron model, τ_r, which represents the time constant of variable r, is much larger than τ_h, and the time constant of the variable h. Then, r is the slow variable and Eqs (2.1a) and (2.1b) are the fast subsystems. First, bifurcations of the fast subsystem are obtained with respect to r. Second, the phase trajectory of the bursting of the whole system (Eqs (2.1a)–(2.1c)) with different I_{app} values are superimposed on the bifurcations of the fast system. Finally, bifurcations related to the beginning and the ending phases of the bursting are identified.

2.4. Methods

In this paper, the fourth-order Runge-Kutta method is used to solve the equations with an integration step of 0.01 ms, and the bifurcation calculations are obtained through MATLAB and its MATCONT subroutine package software [38] .

3. Results

3.1. Electrical behavior of isolated neurons

3.1.1. Resting state, paradoxical bursting, and bifurcations of isolated thalamic neuron

Using I_{app} as the bifurcation parameter, the bifurcation of the TC neuron is obtained, as shown in Figure 2(a). The equilibrium curve is "S" shaped and divided into upper, middle, and lower branches. The lower branch consists of stable nodes (red solid line) and unstable foci (blue dashed line). With the increase of I_{app}, the stable node of the lower branch loses its stability through a subcritical Hopf bifurcation ($SubH_1$, $I_{app} \approx -0.59969\,\mu A/cm^2$). The system undergoes an unstable focus, which then turns into a stable node again through a second subcritical Hopf bifurcation ($SubH_2$, $I_{app} \approx -0.10138\,\mu A/cm^2$). The middle branch consists of saddle points (magenta dashed line). The upper branch consists of the focus. As I_{app} increases, the unstable focus (blue dashed line) is transformed into a stable focus (red solid line) by the supercritical Hopf bifurcation SupH ($I_{app} \approx 39.19564\,\mu A/cm^2$). The stable node of the lower branch meets the saddle point of the middle branch and disappears to form the saddle-node bifurcation SN_1 ($I_{app} \approx 0.56239\,\mu A/cm^2$), which is located in the lower right of Figure 2(a). Additionally, the boundary between the upper and middle branches is the saddle-node bifurcation SN_2 ($I_{app} \approx -1.755587\,\mu A/cm^2$), which is located at the upper left of Figure 2(a). The stable limit cycle emerges via the SupH bifurcation on the upper branch, and between the SupH

($I_{app} \approx 39.19564\,\mu A/cm^2$) and $I_{app} \approx 0.32504\,\mu A/cm^2$; its maximum amplitudes and minimum amplitudes are indicated by the upper and lower green lines, denoted by V_{max} and V_{min}, respectively. The stable limit cycle corresponds to the firing. The two subcritical Hopf bifurcations in the lower branch, $SubH_1$ and $SubH_2$, give birth to two unstable limit cycles (green dashed lines).

Figure 2(b) is a magnification of Figure 2(a) near $I_{app} = 0\,\mu A/cm^2$. At $I_{app} = 0\,\mu A/cm^2$, there is a coexistence of the resting state and stable firing. The upper and lower purple curves indicate the maximum and minimum of the membrane potential corresponding to the firing, which is acquired through a numerical simulation. The parameter region for the coexisting firing is very narrow. Unfortunately, the bifurcation related to the firing and resting states has not been acquired. The electrical activity of the pre-coupled TC neurons studied in this paper at a resting state at $I_{app} = 0\,\mu A/cm^2$.

Unstable limit cycles emerge from both $SubH_1$ and $SubH_2$, as shown by the green dashed curves in Figure 2(b). The unstable limit cycles encounter the saddles on the middle branch to disappear via a saddle-homoclinic orbit bifurcation. Then, an unstable equilibrium point appears between $SubH_1$ and $SubH_2$, as shown by the blue dashed curve on the lower branch. With a numerical simulation, a stable firing between $I_{app} \approx -0.61674\,\mu A/cm^2$ and $I_{app} \approx -0.102\,\mu A/cm^2$ (the upper and lower purple curves correspond to the maximum and minimum values respectively) is acquired. The firing is stable bursting, as shown in Figure 3. Unfortunately, the bifurcations related to the firing and resting states remain unclear. The firing corresponds to a type of paradoxical bursting. There are two reasons for calling it paradoxical bursting. The first reason is that the I_{app} value of the bursting is lower than that of the resting state, thereby suggesting that the bursting is paradoxical, contrary to the traditional notion that an increase in I_{app} induces a firing from the resting state. The second reason is that the number of spikes within a burst decreases as I_{app} decreases, as shown in Figure 3(a)–(d). As I_{app} decreases, the bursting exhibits a period-adding bifurcation, as shown by the interspike intervals (ISIs) in Figure 3(e). The correlation between this paradoxical bursting and the bursting of TC neurons in the network is explained in the following sections.

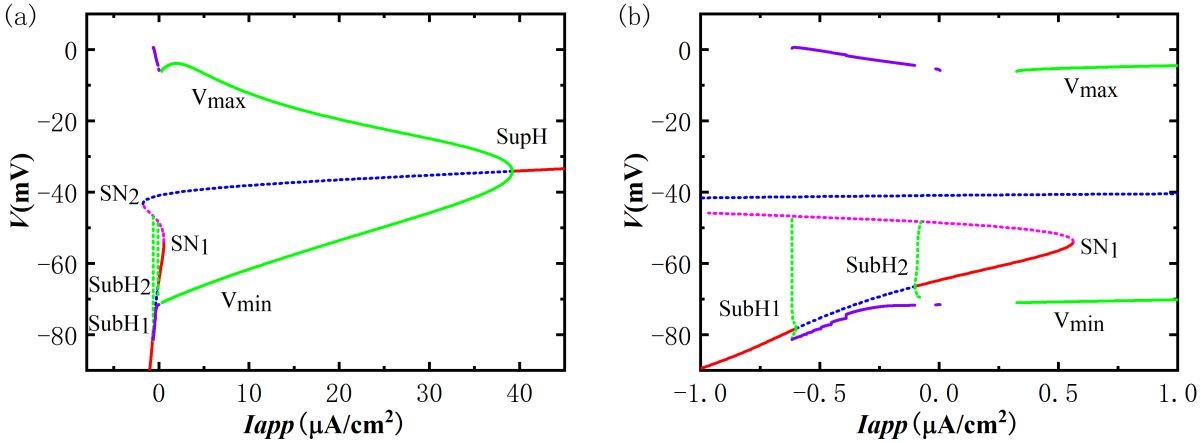

Figure 2. Bifurcations of membrane potential of TC neuron with respect to I_{app}. (a) Global view; (b) Magnification of panel (a) around $I_{app} = 0\,\mu A/cm^2$.The red solid line represents stable node, the blue dashed line represents unstable focus, the purple solid line represents a stable firing corresponds to a type of paradoxical bursting, the green dashed line represents unstable limit cycle, the green solid line represents stable limit cycle, and the magenta dashed line represents saddle points.

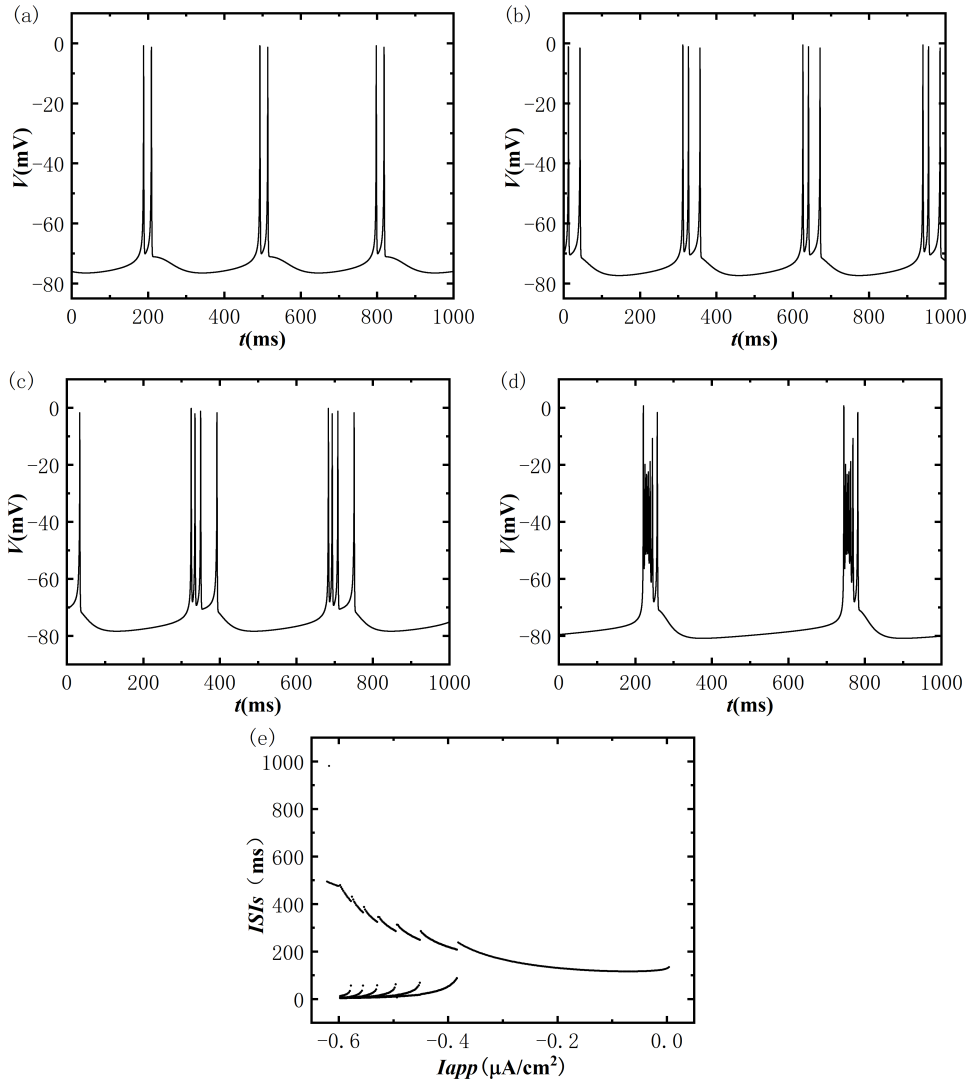

Figure 3. Membrane potentials of TC neuron bursting at different values of I_{app} and bifurcation of ISIs with respect to I_{app}. (a) Period-2 bursting for $I_{app} = -0.45\ \mu A/cm^2$; (b) Period-3 bursting for $I_{app} = -0.47\ \mu A/cm^2$; (c) Period-4 bursting for $I_{app} = -0.5\ \mu A/cm^2$; (d) Period-7 bursting for $I_{app} = -0.61\ \mu A/cm^2$; (e) Bifurcations of ISIs of the bursting with respect to I_{app}.

3.1.2. Electrical activity of isolated STN, GPe and GPi neurons

Figure 4(a) illustrates the bifurcation of the isolated STN neuron influenced by I_{app}. The equilibrium curve presents an "S" shape comprised of the lower branch as stable nodes (solid red line), the middle branch as saddles (illustrated by a magenta dashed line), and the focus on the upper branch. As I_{app} increases, the unstable focus is transformed into a stable focus (solid red line) by a subcritical Hopf bifurcation (SubH, $I_{app} \approx 151.51554\ \mu A/cm^2$). A saddle-node bifurcation on an invariant cycle (SNIC), occurs at $I_{app} \approx -5.45555154\ \mu A/cm^2$(SNIC), via which the stable node from the lower branch meets the saddle from the middle branch. The boundary that separates the middle (saddle) from the upper branch corresponds to a saddle-node bifurcation (SN). This bifurcation occurs at approximately

$-33.83116\,\mu A/cm^2$ of I_{app}.

As I_{app} further increases, an unstable limit cycle emerges around the upper branch (maximum amplitude V_{max} and minimum amplitude V_{min} delineated by upper and lower dashed green lines, respectively) via the SubH bifurcation. Concurrently, a stable limit cycle (solid green lines) also emerges from the SNIC and intersects with the unstable limit cycle. This intersection point forms either a saddle-node or a fold bifurcation of the limit cycle(LPC, $I_{app} \approx -205.01926\,\mu A/cm^2$).

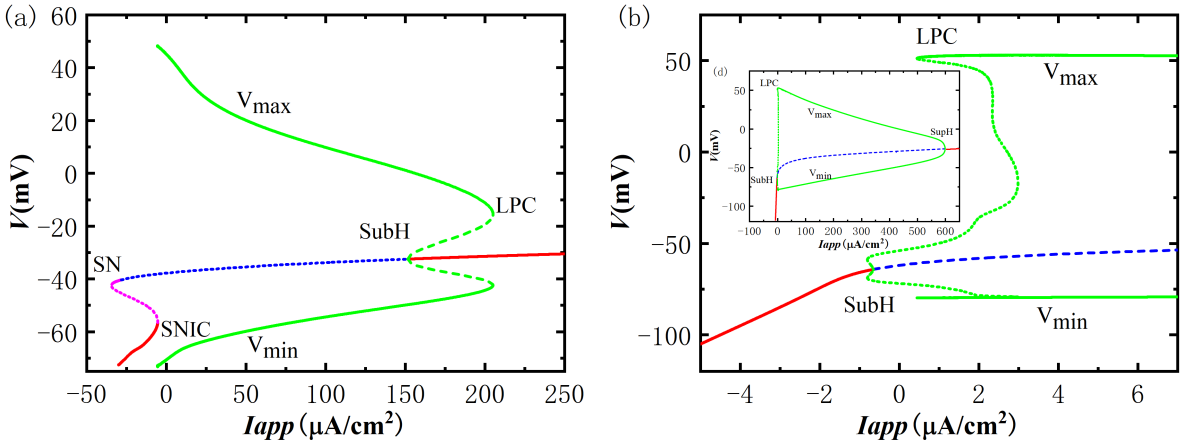

Figure 4. Bifurcations of membrane potentials with respect to I_{app} (a)STN neuron; (b)GPe and GPi neurons (I_{app} in the interval $[-5, 7]$). The insert in the up-left represents the bifurcations over a wide range of I_{app}. The red solid line represents stable node, the blue dashed line represents unstable focus, the green dashed line represents unstable limit cycle, the green solid line represents stable limit cycle, and the magenta dashed line represents saddle points.

Figure 4(b) shows the bifurcations of the GPe and GPi neurons with respect to I_{app}, and the insert panel represents the global view of the bifurcation. The changes of the equilibrium curves are monotonical, which are divided into three segments by the subcritical Hopf bifurcation (SubH, $I_{app} \approx -0.65538\,\mu A/cm^2$) and the supercritical Hopf bifurcation (SupH, $I_{app} \approx 603.4613\,\mu A/cm^2$, shown in the insert panel). The red solid curve represents the stable node and the blue dashed curve represents the unstable focus. As I_{app} changes, the stable limit cycle (green solid line) induced by the SupH bifurcation intersects with the unstable limit cycle (green dashed line) caused by SubH to form the fold bifurcation of limit cycle (LPC, $I_{app} \approx -0.44753\,\mu A/cm^2$).

3.1.3. Firing activity of four types of neurons before coupling

According to the bifurcation diagrams, the neuronal firings before coupling are shown in Figure 5. Figure 5(a) shows the fast-spiking of the STN neuron ($I_{app} = 25\,\mu A/cm^2$), Figure 5(b) shows the spiking of the GPe neuron ($I_{app} = 2.2\,\mu A/cm^2$), Figure 5(c) shows the firing activity of the GPi neuron ($I_{app} = 3\,\mu A/cm^2$), and Figure 5(d) shows the resting state of the TC neuron ($I_{app} = 0\,\mu A/cm^2$). These firing activities are not far from the bifurcation point; therefore, it can be surmised that the complex firing can be evoked when subjected to oscillating synaptic current within the network. When the synaptic current is positive (excitatory), the firing is enhanced; when the synaptic current is negative (inhibitory), the firing is weakened or even stopped, and then bursting may be formed.

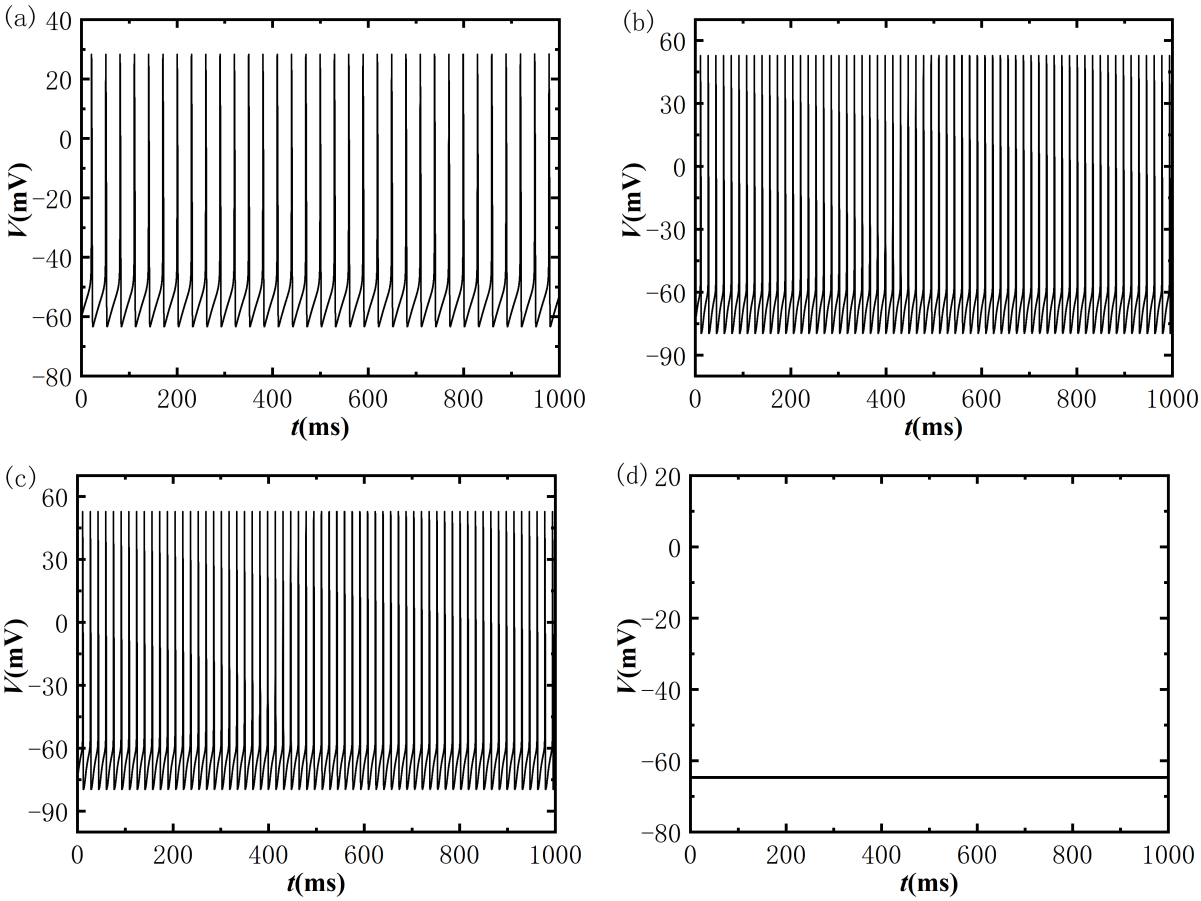

Figure 5. Electrical activities of four types of neurons before coupling (a) Periodic spiking of STN neuron for I_{app} = 25 μA/cm^2; (b) Periodic spiking of GPe neuron for I_{app} = 2.2 μA/cm^2; (c) Periodic spiking of GPi neuron for I_{app} = 3 μA/cm^2; (d) Resting state of TC neuron without cortical input for I_{app} = 0 μA/cm^2.

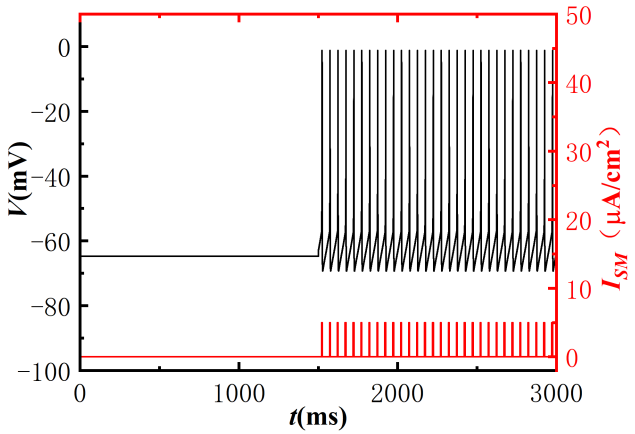

Figure 6. Spiking (t >1500 ms) induced by positive periodic current I_{SM} (red) from the resting state (t <1500 ms) of isolated TC neuron.

3.2. *Electrical behavior of single neurons with external stimulations*

3.2.1. Spiking of thalamic neuron in response to I_{SM}

For the resting state ($I_{app} = 0\,\mu A/cm^2$) of a TC neuron, after being stimulated with a periodic pulse current I_{SM} ($i_{SM} = 5\,\mu A/cm^2$, $\rho_{SM} = 50\,ms$, $\delta_{SM} = 5\,ms$) from the cortex ($t > 1500$ ms), spiking induced by the stimulus pulses is evoked that corresponds to the normal state, as shown in Figure 6. The solid red represents the pulse stimulation. The spiking associated with the limit cycle is shown by the green solid lines in Figure 2(a),(b).

3.2.2. High-frequency electrical activity of STN neurons in response to DBS stimulation

As shown in Figure 7(a), the STN neuron exhibits a fast-spiking state at $I_{app} = 25\,\mu A/cm^2$ ($t <$ 4400 ms). When a high-frequency periodic pulse current I_{DBS}(red, $i_{DBS} = 200\,\mu A/cm^2$, $\rho_{DBS} = 6\,ms$, $\delta_{DBS} = 0.6\,ms$) is applied to stimulate the STN neuron at $t = 4400$ ms, the firing frequency becomes faster. Figure 7(b) is a magnification of Figure 7(a), after which corresponds high-frequency DBS stimulation, the firing frequency of the STN neuron becomes higher, which corresponds to the frequency of I_{DBS}. Within the network, I_{DBS} induced high-frequency spiking of the STN neuron to eliminate bursting of the TC neuron corresponding to PD, which will be investigated in Section 3.3.4.

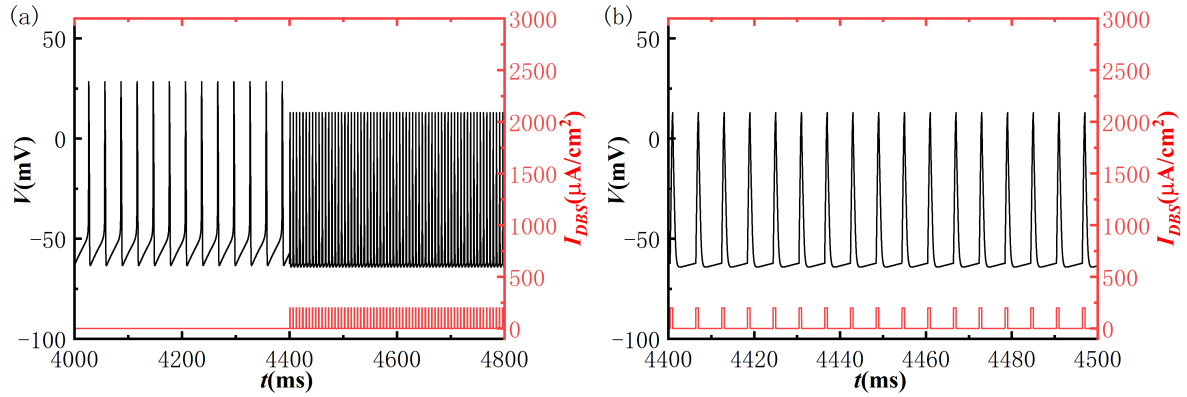

Figure 7. Response of isolated STN neuron to DBS stimulation. (a) Increased frequency of periodic spiking evoked by stimulation I_{DBS} ($i_{DBS} = 200\,\mu A/cm^2$, $\rho_{DBS} = 6\,ms$, $\delta_{DBS} = 0.6\,ms$) applied at $t = 4400$ ms; (b) Magnification of part of the panel (a).

3.2.3. PIR firing of thalamic neuron in response to the inhibitory pulse

A TC neuron at a resting state, receives a negative pulse of 100 ms for a duration of 1000 ms (red), and exhibits a PIR spike (black), as shown in Figure 8. A relatively weak ($-0.195\,\mu A/cm^2$) negative pulse induces a PIR spike, as shown in Figure 8(a), and a relatively strong ($-0.21\,\mu A/cm^2$) negative pulse induces a PIR burst, as shown in Figure 8(b). Obviously, the negative pulse first causes a decrease in the membrane potential; after the end of the stimulation, the membrane potential increases, thereby resulting in a PIR spike. An increase in the membrane potential after the end of the stimulation is caused by the activation of a positive T-calcium current (first decrease and then increase), which is induced by the decrease in membrane potential during the stimulation period, as shown by the green solid line in Figure 8. After the end of the stimulation, the positive T-calcium current continues to exist and increases,

thus causing the membrane potential to rise before the spike or burst.

Therefore, the decrease in membrane potential induced by negative stimulation, which occurs before the PIR spike, is an important feature of the PIR spike. In this paper, we will use this to determine whether the bursting of TC neurons in the network is a PIR spike or not (see Section 3.3.2). The stronger the negative current stimulation is, the larger the positive T-calcium current is. The long decay time caused the burst with more spikes in it, as shown in Figure 8(b). Therefore, the slow-varying factor that determines the generation of bursting is the slow decay of the T-calcium current. Although the TC neurons have the capacity to produce a PIR spike, and TC neurons in the network are also influenced by an inhibitory synaptic current, this paper will reveal that the bursting of the TC neuron in the network corresponding to PD is not a PIR spike (see Figure 9(d),(e)), because the spike is not preceded by a negative pulse.

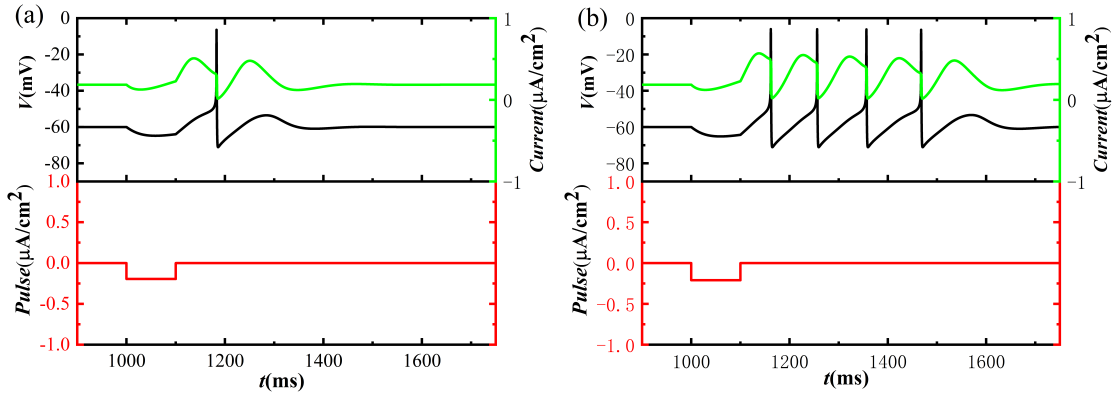

Figure 8. Negative pulse (Duration 100 ms) stimulation induces PIR firing in isolated TC neurons. (a) Weak pulse intensity (-0.195 μA/cm^2) induces a PIR spike; (b) Strong pulse intensity (-0.21 μA/cm^2) induces a PIR burst. The green solid line represents the curve of T-current over time, the red solid line represents the inhibitory pulse current, and black solid line represents the membrane potential of TC neurons.

3.3. Bursting of thalamic neurons in network for Parkinson's disease

3.3.1. Bursting of thalamic neurons and electrical activity of other neurons

Before coupling, STN, GPe and GPi neurons are in spiking (Figure 5), and the TC neuron receiving the corresponding cortical stimulation I_{SM} also exhibits spiking corresponding to the stimulation I_{SM} (Figure 6). The firings of the coupled neurons are shown in Figure 9. The black solid curve represents the neuronal membrane potential, the red solid curve indicates the I_{SM} stimulation received by the thalamic neuron, and the blue solid curve is the inhibitory synaptic current $I_{GPi\to TC}$ from the GPi neuron to thalamic neuron.

Since the STN neuron mainly receives an inhibitory synaptic current from the GPe neuron, STN firing is suppressed to sparse firing, as shown in Figure 9(a). The inhibitory synaptic current is strong in the duration of no spiking (quiescent state). The GPe neuron receives two synaptic currents, which are the inhibitory current of other GPe neurons and the excitatory current of STN neurons. When the inhibitory current is stronger than the excitatory current, the spiking is suppressed to form a quiescent state; when the excitatory current is stronger than the inhibitory current, the firing is enhanced. Then,

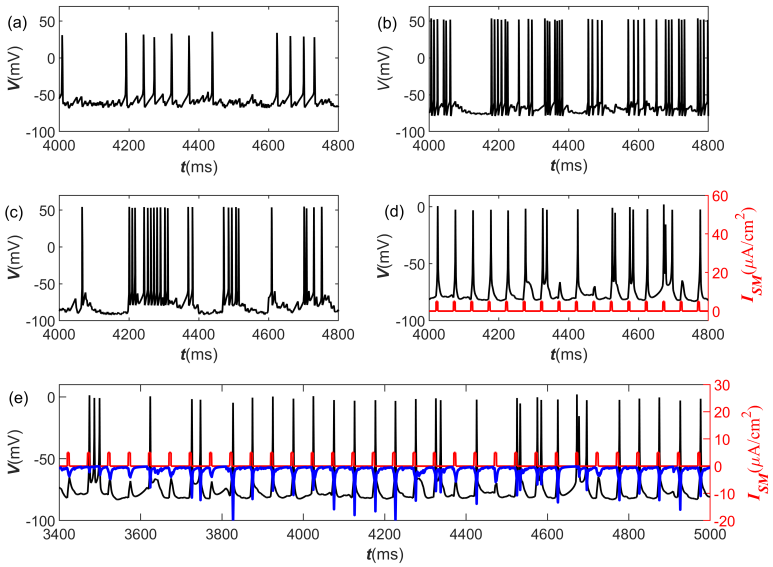

Figure 9. Electrical activities of neurons in the network for PD. (a) STN neuron; (b) GPe neuron; (c) GPi neuron; (d) TC neuron(short time duration); (e) TC neuron(long time duration). The black solid curve represents the membrane potential, the red solid curve denotes the stimulation I_{SM}, and the blue solid curve represents the inhibitory synaptic current received by the TC neuron.

bursting with alternations between the quiescent state and firing appears, as shown in Figure 9(b). GPi neuron is subjected to an inhibitory synaptic current from the GPe neuron and the excitatory current from the STN neuron; similarly, bursting is generated, as shown in Figure 9(c).

In particular, the TC neuron receives an inhibitory synaptic current from the GPi neuron. Under this inhibitory synaptic current, the TC neuron no longer produces spiking in response to each spike of the input current I_{SM} (red), as shown in Figure 9(d),(e) (Figure 9(e) is longer), with the inhibitory synaptic current in blue. At this time, TC neurons respond to the I_{SM} pulse stimulation in three ways:

1) No action potential is generated, as shown in the first stimulation in Figure 9(e), which should be caused by the strong suppression of the inhibitory synaptic current at this time;

2) A Spike is still generated, as shown in the fifth stimulation in Figure 9(e), which is caused by the insufficiently strong inhibitory synaptic current at this time; and

3) Either a double-spike or multiple-spikes bursts are evoked, as depicted in the third stimulation in Figure 9(d),(e). The mechanism for the generation of either a double-spike or multiple-spike bursts is very complex, which has not yet been understood. This is the core of this paper, which is obtained by analyzing the joint action of the inhibitory synaptic current $I_{GPi\to TC}$ and the cortical I_{SM}.

3.3.2. Thalamic bursting is not PIR bursting

The amplification of the bursting and inhibitory synaptic current in Figure 9(e) is shown in Figure 10(a). Corresponding to the action potential, the inhibitory synaptic current generates a large negative pulse, which is due to the expression of the synaptic current as $I_{GPi\to TC} = g_{GPi\to TC}(V_{TC} - E_{GPi\to TC}) \sum_j s^j_{GPi}$.

Therefore, when the postsynaptic membrane potential V_{TC} (action potential of TC neuron) is higher, then a stronger synaptic current is received by the postsynaptic neuron, because the size of synaptic current is related to V_{TC} . The fact is that the large negative synaptic current pulse does not precede the action potential; moreover, it indicates that the spikes are not caused by the negative synaptic current. On the contrary, the negative synaptic current pulse is caused by the action potential. Therefore, the bursting is not PIR bursting.

The blue and red colors in Figure 10(b) are the inhibitory synaptic current and the I_{SM} stimulation, respectively. It can be found that, except for the large negative synaptic current pulse corresponding to the action potential, the blue pulse corresponding to a I_{SM} below the black dashed line ($-2\ \mu A/cm^2$), the inhibitory synaptic current between the neighboring red pulse is weaker than that the black dashed line, $-2\ \mu A/cm^2$, for most of the time, as shown in Figure 10(b). Therefore, two speculations can be made. One is that the bursting of TC neurons should be generated by the combined effect of a relatively weak inhibitory synaptic current and a positive pulse I_{SM}, which will be illustrated by the response of isolated TC neurons to an external negative stimulation and a positive pulse (see Section 3.3.2); and the other is the elimination of the inhibitory synaptic current can induce spiking of TC neurons in response to the I_{SM} pulses recovered, which will be illustrated by the DBS stimulation to eliminate an inhibitory synaptic current to recover the spiking of TC neurons by removing the inhibitory synaptic current (see Section 3.3.4).

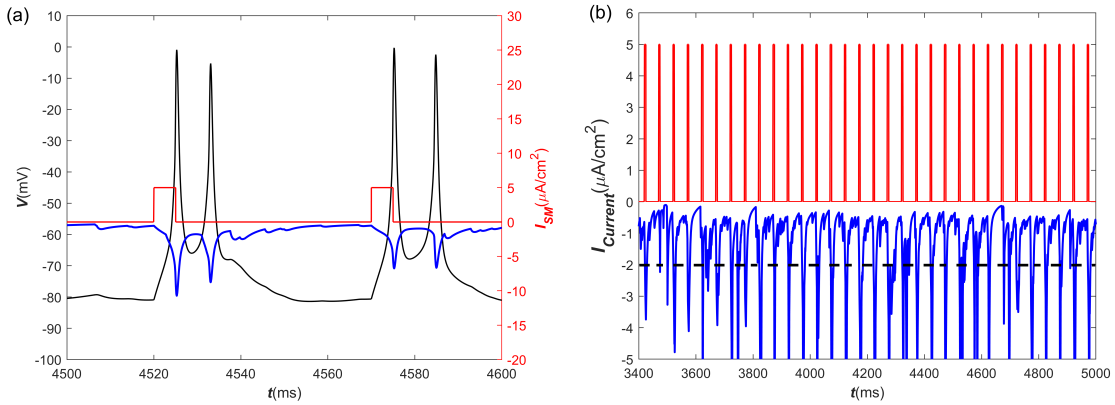

Figure 10. Relationship between burst of TC neuron in network and inhibitory synaptic current received by the TC neuron for PD. (a) Membrane potential (black), I_{SM} (red), and inhibitory synaptic current (blue); (b) I_{SM} (red) and inhibitory synaptic current (blue). The inhibitory current pulses below the black dashed line are caused by the peak of action potentials.

3.3.3. Thalamic bursting is caused by both inhibitory current and I_{SM}

The results in Figure 11 corroborate that the bursting of the thalamic neuron within the network is induced by the combined action of an inhibitory synaptic current and an excitatory pulse current ($i_{SM} = 5\ \mu A/cm^2$, $\rho_{SM} = 50$ ms, $\delta_{SM} = 5$ ms). A thalamic neuron stimulated with $I_{app} = 0\ \mu A/cm^2$ exhibits spiking, as shown in Figure 11(a). Currents of $-1\ \mu A/cm^2$ and $-1.3\ \mu A/cm^2$ are selected to simulate an inhibitory synaptic current weaker than $-2\ \mu A/cm^2$. The introduction of a negative current of $-1\ \mu A/cm^2$ (as shown by the blue solid line in Figure 11(b)) to Figure 11(a) induces bursting, as shown in Figure 11(b), and the introduction of a negative current of $-1.3\ \mu A/cm^2$ (as shown by the blue

solid line in Figure 11(c)) to Figure 11(a) also causes a bursting, as shown in Figure 11(c). The negative currents in Figure 11(b),(c) correspond to the inhibitory synaptic current in Figure 10(b). Therefore, the bursting of TC neurons that correspond to PD is induced by an inhibitory current. Considering that the paradoxical bursting in Figure 3 is also induced by a negative current, the bursting of TC neurons in the network that correspond to PD also correspond to the paradoxical bursting of TC neurons.

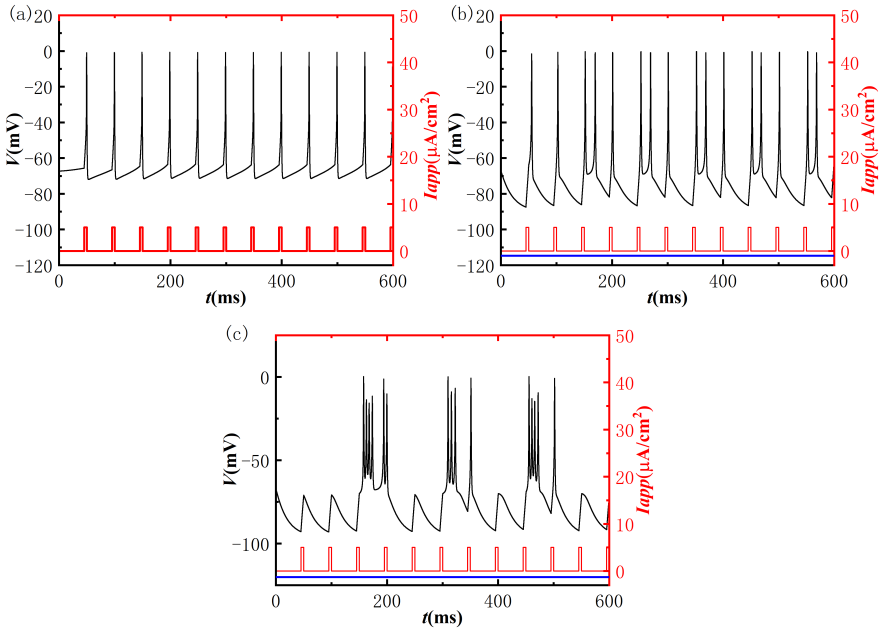

Figure 11. Inhibitory current and I_{SM} together evoke bursts of TC neuron. (a) One-to-one spikes induced by I_{SM}; (b) Negative current with amplitude -1 μA/cm^2 (blue) introduced to (a) induces burst; (c) Negative current with amplitude -1.3 μA/cm^2 (blue) introduced to (a) induces burst. Black denotes membrane potential, and red represents I_{SM}.

3.3.4. DBS stimulation remove thalamic bursting to recover normal firing

The results shown in Figure 12 confirm another speculation proposed in Section 3.3.1, that removing inhibitory synaptic currents can eliminate bursting of the TC neuron and restore the spiking corresponding to the pulses I_{SM} (blue solid lines). For the state corresponding to PD shown in Figure 9, a DBS current is applied to each STN neuron in the network, as shown in Figure 12(a), with the black solid curve representing the neuron membrane potential and the red solid curve denoeting I_{DBS}. Under the high-frequency stimulation I_{DBS}, the STN neurons become high-frequency spiking, as shown in Figure 12(a),(e); Figure 12(e) is a magnification of Figure 12(a). The high spiking frequency of the STN neuron causes the excitatory effect from the STN neuron to the GPe neuron enhanced. Then, the GPe neuron's spiking enhances and the spiking frequency increases, as shown in Figure 12(b),(f); the magnification of Figure 12(b) is shown in Figure 12(f). Each GPi neuron receives an inhibitory effect from two GPe neurons and an excitatory effect from one STN neuron. Then, the inhibitory effect of the GPe neuron becomes strong, which makes the activities of the GPi neurons either weak or nonexistent to become resting state, as shown in Figure 12(c). Therefore, the inhibitory synaptic current from the GPi neuron to the TC neuron is either weak or nonexistent, and Figure 12(d) corresponds to the disappearance of the inhibitory synaptic current. At this time, the TC neuron only receives I_{SM} stimulation and recovers

spiking in response to the I_{SM} current, which corresponds to the normal state. This suggests that DBS stimulation is a treatment measure for PD.

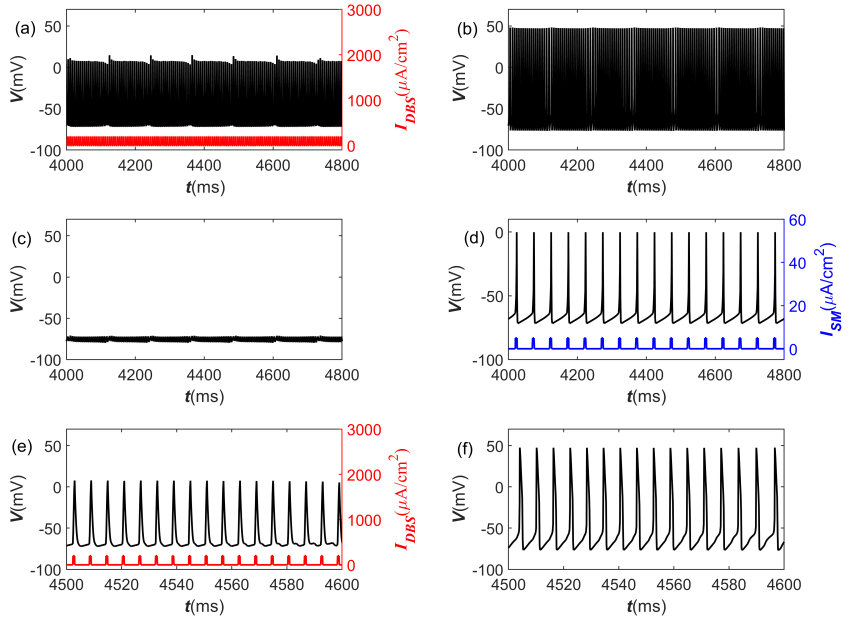

Figure 12. Application of DBS stimulation to STN neurons (red solid line) induces changes in the electrical activities of neurons within the network. (a) High-frequency firing of the STN neuron; (b) High-frequency firing of the GPe neuron; (c) Resting state of the GPi neuron; (d) Firing of TC neuron recovers to one-to-one spikes induced by pulse (blue solid line); (e) Enlargement of panel (a); (f) Enlargement of panel (b).

3.4. Fast-slow dynamics of paradoxical bursting in isolated thalamic neuron

The paradoxical bursting of a thalamic neuron in the network related to PD is matched by a similar bursting (i.e., the paradoxical bursting) in an isolated thalamic neuron. In this section, the fast-slow dynamic of the four bursting patterns depicted in Figure 3 is analyzed. In the equilibrium bifurcation of the first kind of bursting (as shown in Figure 3(a) featured in Figure 13(a)), an exemplified "Z"-shaped equilibrium curve is divided into three parts: the upper, middle, and lower branches. The upper branch is made up of the focus. With the steady rise of the bifurcation parameter, the unstable focus (black dashed line) morphs into a stable focus (red solid line) via a supercritical Hopf bifurcation (SupH, $r \approx -0.15645$). The saddle point (blue dashed line) characterizes the middle branch while the lower branch is formed by the stable node (red solid line). Both the lower and middle branches intersect to create a saddle-node bifurcation (SN_2 at $r \approx 0.19231$)(i.e., a fold bifurcation), with another saddle-node bifurcation (SN_1, $r \approx -0.00605$) formed by the intersection of the upper and middle branches. An upper branch-emerging stable limit cycle is introduced (The maximum amplitude V_{max} and minimum amplitude V_{min} are indicated by the upper and lower green lines, respectively), via the SupH bifurcation. This stable limit cycle coincides with the saddle point on the middle branch to produce a saddle-homoclinic orbit (SH) bifurcation ($r \approx 0.06868$) as the bifurcation parameter decreases. An overlying

phase trajectory of the bursting (purple solid line) on Figure 13(b) leads to Figure 13(c). Figure 13(d)–(f) similarly detail the dissection results of the bursting from Figure 3(b)–(d), each in regards to fast-slow variable, respectively.

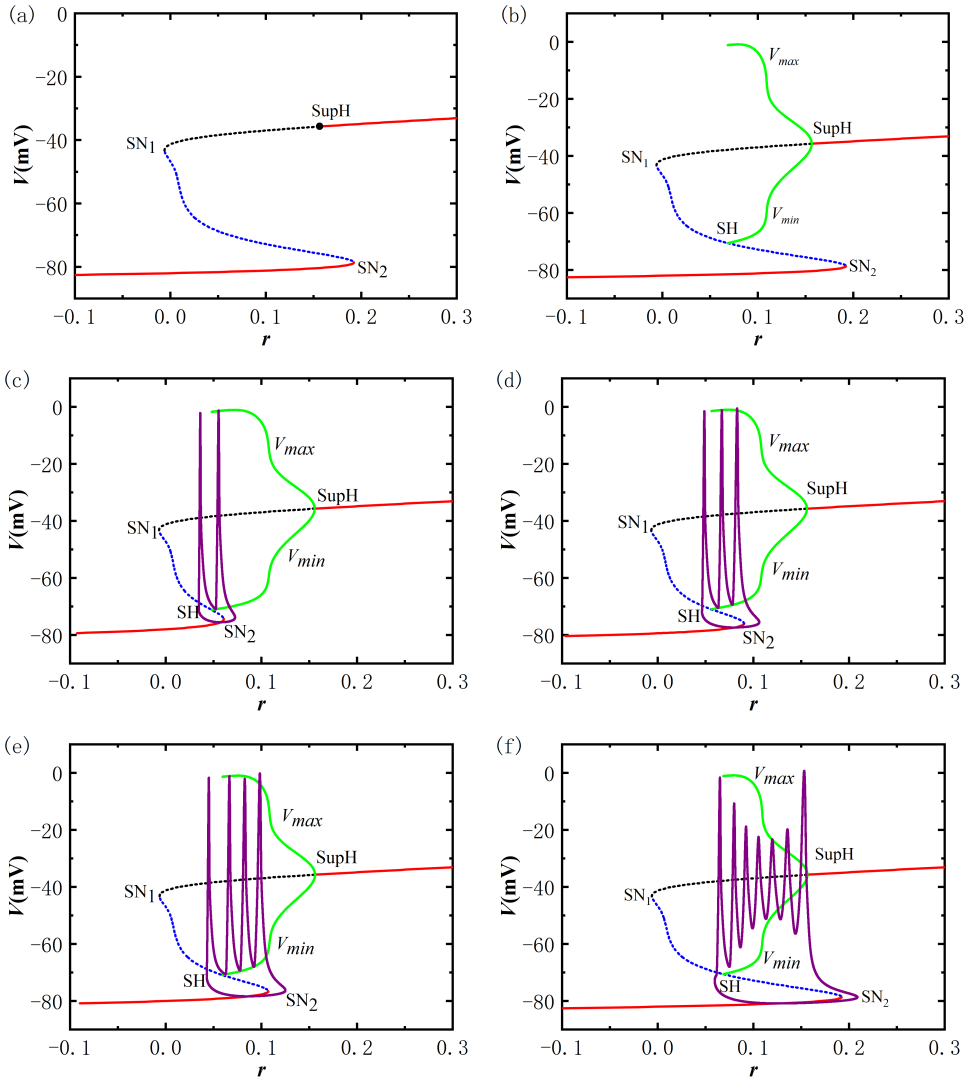

Figure 13. Fast-slow dynamics of paradoxical burst of TC neuron (a) Bifurcations of equilibrium points of fast subsystem for $I_{app} = -0.61$ μA/cm^2; (b) Bifurcations of equilibrium points and limit cycle (Green) of fast subsystem for $I_{app} = -0.61$ μA/cm^2; (c) Phase trajectory of bursting for $I_{app} = -0.61$ μA/cm^2 superimposed on panel (b); (d) Fast-slow dynamics of period-3 bursting for $I_{app} = -0.5$ μA/cm^2; (e) Fast-slow dynamics of period-4 bursting for $I_{app} = -0.47$ μA/cm^2; (f) Fast-slow dynamics of period-7 bursting for $I_{app} = -0.45$ μA/cm^2.

The first spikes in the bursting in Figure 13(c)–(f) start at the SN bifurcation(i.e., a fold bifurcation), and the phase trajectories jump from the lower branch to the stable limit cycle, and then become spiking around the stable limit cycle. After two or more spikes, the phase trajectories reach the homoclinic (SH) bifurcation to jump down to the stable node in the lower branch, and a period of burst is completed. Therefore, the burst begins at the fold (SN) bifurcation and ends at the homoclinic (SH) bifurcation,

resulting in the "Fold/Homoclinic" bursting. This result is different from the results of other models of thalamic neurons in the literature [39], wherein the fast subsystem produces a saddle-node bifurcation on an invariant cycle. This suggests a future comprehensive study of different thalamic models of neurons.

4. Discussion and conclusions

The pathogenesis and treatment of PD have been extensively studied in experimental and theoretical models [5–12]. The basal ganglia regulates the electrical activity of the thalamus, and bursting of TC neuron is one of its manifestations. Through DBS of different nuclei of the basal ganglia, such as the subthalamic nucleus, bursting can be eliminated to restore normal firing, which can effectively used to treat PD [4,40,41]. Although there have been numerous studies conducted, the exact mechanism behind the generation and elimination of thalamic bursting remains unclear, due to various responses under excitatory and inhibitory modulation [21,28,29,42,43]. In this paper, we investigated the nonlinear dynamics of generation and elimination of PD-related thalamic bursting [8]. By identifying different responses under excitatory and inhibitory modulation, and combining them with a number of existing electrophysiological experiments [5,14,44–47], the following conclusions were obtained.

First, the single thalamic neuron exhibits paradoxical bursting, which refers to the phenomenon that inhibitory effects induce bursting from a resting state. This contradicts the traditional belief that inhibitory effects suppress the firing activity, hence being named "paradoxical bursting". In this paper, we utilized a thalamic neuron model that was extensively documented in the existing literature [8]; through a bifurcation analysis and a numerical simulation, we found that the bursting phenomenon can be triggered from a resting state by reducing the transmembrane current from 0. The occurrence of paradoxical bursting, as well as the occurrence of recent paradoxical bursting triggered by enhanced excitatory/inhibitory effects [18,48], offer valuable insights into bursting dynamics and excitatory/inhibitory modulations.

Second, an isolated thalamic neuron possesses the capability to generate post-inhibitory rebound bursting when subjected to an inhibitory pulse stimulus. However, the bursting behavior of thalamic neurons within a network is not characterized by rebound bursting. At a resting state of the thalamic neuron, the application of an inhibitory pulse stimulation activates the positive T-type calcium current to trigger a PIR, which corresponds to the rebound firing found in experimental studies [18]. Rebound firing represents a significant paradoxical electrical activity of the nervous system [48,49], and its relationship with epilepsy and PD has been well-established [5,15,25,50,51]. This contradicts the conventional understanding that inhibitory effects suppress firing. One necessary characteristic of the rebound spike is that the incoming inhibitory pulse stimulation should precede the rebound itself. However, in the network examined in this study, the inhibitory synaptic current pulse appears after the spike or burst, thereby leading to the conclusion that the bursting of thalamic neurons in this context is not rebound bursting.

Finally, the bursting of thalamic neurons in the network associated with PD is a paradoxical form of bursting initiated by the inhibitory synaptic current. However, a DBS applied to the STN eliminates the inhibitory synaptic current received by the thalamic neuron, thus resulting in the restoration of a regular spiking pattern. In the normal state, the thalamic neuron faithfully responds to the excitatory input from the cortex I_{SM}. Within the network, the frequency of STN spiking is reduced by the inhibitory effect of GPe. Therefore, the firing with high frequency changes to bursting alternating between a quiescent state

(inhibitory effect is strong) and burst (exciatory effect is strong). GPi inhibitory synapses to the thalamic neurons also exhibit time-varying properties. As a result, there are three types of firing response to a pulse: no spiking, spiking, and bursting. The former two scenarios are easily understood because the inhibitory synaptic current is either strong enough to suppress the spiking or is not strong enough to affect the spiking. However, the last scenario, in which the inhibitory effect induces a bursting, has been difficult to be understand up to now. The present study reveals that the bursting is a paradoxical bursting induced by the inhibitory synaptic current from the basal ganglia, which presents a plausible theoretical explanation for the thalamic bursting. When a DBS stimulation is applied, the STN firing rate is increased, the activity of GPe is enhanced, and GPi is inhibited by the enhanced GPe; thus, the electrical activity of GPi is weakened or even becomes the resting state. Then, the inhibitory synaptic current to the thalamus either reduces or disappears, and the thalamus resumes simple spiking corresponding to normal state. This result reveals the principle of DBS stimulation in the treatment of PD at the level of network, which is the interrelationship between the excitatory and inhibitory modulations to electrical activities of the nuclei in the basal ganglia. In the future, we can continue to study the mechanism of DBS stimulation of other nuclei, such as GPe, in the treatment of PD.

By elucidating the intricate and paradoxical nonlinear dynamics of individual neurons and the complex dynamics of the network influenced by both excitatory and inhibitory effects, this research offers a new theoretical comprehension of the mechanisms underlying the emergence and disappearance of thalamic bursting in PD. The bursting activity observed is a result of paradoxical behavior induced by inhibitory modulation rather than by rebound bursting. The amplification of spiking activity in the thalamic nucleus can decrease the inhibitory synaptic current originating from the GPi to the thalamus and eliminate the paradoxical bursting, thereby yielding therapeutic effects. Our findings contribute to the expansion of examples of paradoxical nonlinear phenomena, improve our understanding of inhibitory regulation, and propose a new mechanism underlying thalamic bursting in PD. In the future, bursting related to PD should be studied in multiple thalamic models and network models containing more parts related to PD, with more modulations being considered.

Use of AI tools declaration

The authors declare they have not used Artificial Intelligence (AI) tools in the creation of this article.

Acknowledgments

This work is supported by National Natural Science Foundation of China (No. 12072236), Postgraduate Education Reform and Quality Improvement Project of Henan Province (No. YJS2023SZ15), and The key program of Henan province higher education (No. 24A110005).

Conflict of interest

The authors declare there is no conflicts of interest.

References

1. M. M. McGregor, A. B. Nelson, Circuit mechanisms of Parkinson's disease, *Neuron*, **101** (2019), 1042–1056. https://doi.org/10.1016/j.neuron.2019.03.004
2. M. M. McGregor, A. B. Nelson, Directly to the point: dopamine persistently enhances excitability of direct pathway striatal neurons, *Neuron*, **106** (2020), 201–203. https://doi.org/10.1016/j.neuron.2020.04.005
3. P. Zhao, B. Zhang, Y. Xiao, P. Kong, F. Sun, Therapeutic effect observation of selegiline hydrochloride in early stage of Parkinson's disease, *J. Clin. Neurol.*, **18** (2005), 306–307. https://doi.org/10.3969/j.issn.1004-1648.2005.04.023
4. M. Jakobs, D. J. Lee, A. M. Lozano, Modifying the progression of Alzheimer's and Parkinson's disease with deep brain stimulation, *Neuropharmacology*, **171** (2020), 107860. https://doi.org/10.1016/j.neuropharm.2019.107860
5. J. Kim, Y. Kim, R. Nakajima, Inhibitory basal ganglia inputs induce excitatory motor signals in the thalamus, *Neuron*, **95** (2017), 1181–1196. https://doi.org/10.1016/j.neuron.2017.08.028
6. Y. Yu, F. Han, Q. Wang, Q. Wang, Model-based optogenetic stimulation to regulate beta oscillations in Parkinsonian neural networks, *Cognit. Neurodyn.*, **16** (2022), 667–681. https://doi.org/10.1007/s11571-021-09729-3
7. Y. Yu, X. Wang, Q. Wang, Q. Wang, A review of computational modeling and deep brain stimulation: applications to Parkinson's disease, *Appl. Math. Mech.*, **41** (2020), 1747–1768. https://doi.org/10.1007/s10483-020-2689-9
8. D. Terman, J. E. Rubin, A. C. Yew, C. J. Wilson, Activity patterns in a model for the subthalamopallidal network of the basal ganglia, *J. Neurosci.*, **22** (2002), 2963–2976. https://doi.org/10.1523/JNEUROSCI.22-07-02963.2002
9. J. E. Rubin, D. Terman, High frequency stimulation of the subthalamic nucleus eliminates pathological thalamic rhythmicity in a computational model, *J. Comput. Neurosci.*, **16** (2004), 211–235. https://doi.org/10.1023/B:JCNS.0000025686.47117.67
10. R. Q. So, A. R. Kent, W. M. Grill, Relative contributions of local cell and passing fiber activation and silencing to changes in thalamic fidelity during deep brain stimulation and lesioning: a computational modeling study, *J. Comput. Neurosci.*, **32** (2012), 499–519. https://doi.org/10.1007/s10827-011-0366-4
11. Y. Yu, F. Han, Q. Wang, Exploring phase-amplitude coupling from primary motor cortex-basal ganglia-thalamus network model, *Neural Networks*, **153** (2022), 130–141. https://doi.org/10.1016/j.neunet.2022.05.027
12. H. A. Braun, H. Wissing, K. Schafer, M. C. Hirsch, Oscillation and noise determine signal transduction in shark multimodal sensory cells, *Nature*, **367** (1994), 270–273. https://doi.org/10.1038/367270a0
13. H. Gu, B. Pan, G. Chen, L. Duan, Biological experimental demonstration of bifurcations from bursting to spiking predicted by theoretical models, *Nonlinear Dyn.*, **78** (2014), 391–407. https://doi.org/10.1007/s11071-014-1447-5

14. H. Gu, B. Pan, Identification of neural firing patterns, frequency and temporal coding mechanisms in individual aortic baroreceptors, *Front. Comput. Neurosci.*, **9** (2015). https://doi.org/10.3389/fncom.2015.00108

15. Y. Yang, Y. Cui, K. Sang, Y. Dong, Z. Ni, S. Ma, et al., Ketamine blocks bursting in the lateral habenula to rapidly relieve depression, *Nature*, **554** (2018), 317–322. https://doi.org/10.1038/nature25509

16. E. M. Izhikevich, Neural excitability, spiking and bursting, *Int. J. Bifurcation Chaos*, **10** (2000), 1171–1266. https://doi.org/10.1142/S0218127400000840

17. L. Duan, W. Liang, W. Ji, H. Xi, Bifurcation patterns of bursting within pre-Bötzinger complex and their control, *Int. J. Bifurcation Chaos*, **30** (2020), 2050192. https://doi.org/10.1142/S0218127420501928

18. Y. Jiang, B. Lu, W. Zhang, H. Gu, Fast autaptic feedback induced-paradoxical changes of mixed-mode bursting and bifurcation mechanism, *Acta Phys. Sin.*, **70** (2021), 170501. https://doi.org/10.7498/aps.70.20210208

19. Y. Liang, B. Lu, H. Gu, Analysis to dynamics of complex electrical activities in Wilson model of brain neocortical neuron using fast-slow variable dissection with two slow variables, *Acta Phys. Sin.*, **71** (2022), 230502. https://doi.org/10.7498/aps.71.20221416

20. B. Lu, H. Gu, X. Wang, H. Hua, Paradoxical enhancement of neuronal bursting response to negative feedback of autapse and the nonlinear mechanism, *Chaos, Solitons Fractals*, **145** (2021), 110817. https://doi.org/10.1016/j.chaos.2021.110817

21. A. Destexhe, M. Neubig, D. Ulrich, J. Huguenard, Dendritic low-threshold calcium currents in thalamic relay cells, *J. Neurosci.*, **18** (1998), 3574–3588. https://doi.org/10.1523/JNEUROSCI.18-10-03574.1998

22. J. M. Goaillard, A. L. Taylor, S. R. Pulver, E. Marder, Slow and persistent postinhibitory rebound acts as an intrinsic short-term memory mechanism, *Phys. Rev. Lett.*, **30** (2010), 4687–4692. https://doi.org/10.1523/JNEUROSCI.2998-09.2010

23. R. Felix, A. Fridberger, S. Leijon, A. S. Berrebi, Sound rhythms are encoded by postinhibitory rebound spiking in the superior paraolivary nucleus, *J. Neurosci.*, **31** (2011), 12566–12578. https://doi.org/10.1523/JNEUROSCI.2450-11.2011

24. K. Ma, H. Gu, Y. Jia, The neuronal and synaptic dynamics underlying post-inhibitory rebound burst related to major depressive disorder in the lateral habenula neuron model, *Cognit. Neurodyn.*, **2023** (2023). https://doi.org/10.1007/s11571-023-09960-0

25. W. M. Howe, P. J. Kenny, Burst firing sets the stage for depression, *Nature*, **554** (2018), 304–305. https://doi.org/10.1038/d41586-018-01588-z

26. K. Chen, L. Aradi, N. Thon, M. Ahmadi, Persistently modified h-channels after complex febrile seizures convert the seizure-induced enhancement of inhibition to hyperexcitability, *Nat. Med.*, **7** (2001), 331–337. https://doi.org/10.1038/85480

27. M. Chang, J. A. Dian, S. Dufour, L. Wang, H. M. Chameh, M. Ramani, et al., Brief activation of GABAergic interneurons initiates the transition to ictal events through post-inhibitory rebound excitation, *Neurobiol. Dis.*, **109** (2018), 102–116. https://doi.org/10.1016/j.nbd.2017.10.007

28. A. Destexhe, T. Bal, D. A. Mccormick, T. J. Sejnowski, Ionic mechanisms underlying synchronized oscillations and propagating waves in a model of ferret thalamic slices, *J. Neurophysiol.*, **76** (1996), 2049–2070. https://doi.org/10.1152/jn.1996.76.3.2049

29. A. Destexhe, T. J. Sejnowski, The initiation of bursts in thalamic neurons and the cortical control of thalamic sensitivity, *Phil. Trans. R. Soc. B*, **357** (2002), 1649–1657. https://doi.org/10.1098/rstb.2002.1154

30. B. Cao, L. Guan, H. Gu, Bifurcation mechanism of not increase but decrease of spike number within a neural burst induced by excitatory effect, *Acta Phys. Sin.*, **67** (2018), 240502. https://doi.org/10.7498/aps.67.20181675

31. H. Hua, B. Lu, H. Gu, Nonlinear mechanism of excitatory autapse-induced reduction or enhancement of firing frequency of neuronal Bursting, *Acta Phys. Sin.*, **69** (2020), 090502. https://doi.org/10.7498/aps.69.20191709

32. Y. Yang, Y. Li, H. Gu, Nonlinear mechanisms for opposite responses of bursting activities induced by inhibitory autapse with fast and slow time scale, *Nonlinear Dyn.*, **111** (2023), 7751–7772. https://doi.org/10.1007/s11071-023-08229-9

33. X. Wang, H. Gu. Y. Jia, Nonlinear mechanism for enhanced and reduced bursting activity respectively induced by fast and slow excitatory autapse, *Chaos, Solitons Fractals*, **116** (2023), 112904. https://doi.org/10.1016/j.chaos.2022.112904

34. X. Wang, H. Gu, Post inhibitory rebound spike related to nearly vertical nullcline for small homoclinic and saddle-node bifurcations, *Electron. Res. Arch.*, **30** (2022), 459–480. https://doi.org/10.3934/era.2022024

35. B. Lu, S. Liu, X. Liu, X. Jiang, Bifurcation and spike adding transition in Chay-Keizer Model, *Int. J. Bifurcation Chaos*, **26** (2016), 1650090. https://doi.org/10.1142/S0218127416500905

36. B. Lu, X. Jiang, Reduced and bifurcation analysis of intrinsically bursting neuron model, *Electron. Res. Arch.*, **31** (2023), 5928–5945. https://doi.org/10.3934/era.2023301

37. E. M. Izhikevich, *Dynamical Systems in Neuroscience: The Geometry of Excitability and Bursting*, MIT Press, 2006. https://doi.org/10.7551/mitpress/2526.001.0001

38. A. Dhooge, W. Govaerts, Y. A. Kuznetsov, MATCONT: a Matlab package for numerical bifurcation analysis of ODEs, *ACM Trans. Math. Software*, **29** (2003), 141–164. http://dx.doi.org/10.1145/779359.779362

39. M. E. Rush, J. Rinzel, Analysis of bursting in a thalamic neuron model, *Biol. Cybern.*, **71** (1994), 281–291. https://doi.org/10.1007/BF00239616

40. S. Li, G. W. Arbuthnott, M. J. Jutras, J. A. Goldberg, D. Jaeger, Resonant antidromic cortical circuit activation as a consequence of high-frequency subthalamic deep-brain stimulation, *J. Neurophysiol.*, **98** (2007), 3525–3527. https://doi.org/10.1152/jn.00808.2007

41. X. Shi, Z. Zhang, Multiple-site deep brain stimulation with delayed rectangular waveforms for Parkinson's disease, *Electron. Res. Arch.*, **29** (2021), 3471–3487. https://doi.org/10.3934/era.2021048

42. D. A. McCormick, H. R. Feeser, Functional implications of burst firing and single spike activity in lateral geniculate relay neurons, *Neuroscience*, **39** (1990), 103–113. https://doi.org/10.1016/0306-4522(90)90225-s

43. X. Shi, D. Du, Y. Wang, Interaction of indirect and hyperdirect pathways on synchrony and tremor-related oscillation in the basal ganglia, *Neural Plast.*, **2021** (2021), 6640105. https://doi.org/10.1155/2021/6640105

44. E. Cheong, Y. Zheng, K. Lee, H. S. Shin, Deletion of phospholipase C β 4 in thalamocortical relay nucleus leads to absence seizures, *PNAS*, **106** (2009), 21912–21917. https://doi.org/10.1073/pnas.0912204106

45. M. Wang, J. Wang, Dynamical balance between excitation and inhibition of feedback neural circuit via inhibitory synaptic plasticity, *Acta Phys. Sin.*, **64** (2015), 108701. https://doi.org/10.7498/aps.64.108701

46. A. Lahiri, M. Bevan, Dopaminergic transmission rapidly and persistently enhances excitability of D1 receptor-expressing striatal projection neurons, *Neuron*, **106** (2020), 227–290. https://doi.org/10.1016/j.neuron.2020.01.028

47. T. A. Spix, S. Nanivadekar, N. Toong, L. M. Kaplow, B. R. Lsett, Y. Goksen, et al., Population-specific neuromodulation prolongs therapeutic benefits of deep brain stimulation, *Science*, **374** (2021), 201–206. https://doi.org/10.1126/science.abi7852

48. X. Wang, H. Gu, Y. Jia, B. Lu, H. Zhou, Bifurcations for counterintuitive post-inhibitory rebound spike related to absence epilepsy and Parkinson disease, *Chin. Phys. B*, **32** (2023), 090502. https://doi.org/10.1088/1674-1056/acd7d3

49. X. Wang, H. Gu, Y. Jia, Relationship between threshold and bifurcations for paradoxical firing responses along with seizure induced by inhibitory stimulation, *Europhys. Lett.*, **142** (2023), 50002. https://doi.org/10.1209/0295-5075/acd474

50. M. Nejad, S. Rotter, R. Schmidt, Basal ganglia and cortical control of thalamic rebound spikes, *Eur. J. Neurosci.*, **54** (2021), 4295–5313. https://doi.org/10.1111/ejn.15258

51. D. Kim, I. Song, S. Keum, T. Lee, Lack of the burst firing of thalamocortical relay neurons and resistance to absence seizures, *Neuron*, **31** (2001), 35–45. https://doi.org/10.1016/0306-4522(90)90225-s

AIMS Press